Nanoscale Advances

ROYAL SOCIETY OF CHEMISTRY

PAPER

View Article Online
View Journal | View Issue

Cite this: *Nanoscale Adv.*, 2025, **7**, 3267

Folate receptor-targeted pH-sensitive liposomes loaded with TGX-221 against prostate cancer by inhibiting PI3K/110β signaling†

Weibo Xu,‡[ad] Xiaohan Li,‡[b] Fujin He,‡[b] Han Zhao,[b] Jing Wu,[b] Mengyu Li,[b] Xiaoying Dai,[b] Yanmin Li,[b] Xiaojiao Hu,[b] Xiaodong Li,[d] Juan Cen,*[bc] Peng Guo*[a] and Shaofeng Duan *[bc]

Prostate cancer (PCa) is the most common cancer in men and the leading cause of cancer death worldwide. Overactivation of PI3K signaling has been reported to be associated with PCa. TGX221 is an effective specific inhibitor of PI3K, but its clinical application is greatly limited due to its poor solubility. Herein, by using folic acid-PEG-cholesterol semi-succinate (FA-PEG-CHEMS) as the targeting component, we developed a folate receptor-targeted pH-sensitive liposomal delivery system loaded with TGX221 (FA-Lip-TGX221) that could realize effective delivery and controlled release of drugs in the tumor. The prepared liposomes exhibited a uniform particle size and high stability. In addition, FA-Lip-TGX221 could be effectively internalized by PC-3 cells due to its ability to target folate receptors, thereby accumulating in tumor tissues. Meanwhile, *in vitro* and *in vivo* experiments suggested that FA-Lip-TGX221 could activate the PERK-ATF4-CHOP signaling pathway by inhibiting PI3K/110β signaling in PCa, thus significantly promoting endoplasmic reticulum (ER) stress-mediated cancer cell death. In conclusion, FA-Lip-TGX221 is a promising nano-delivery vehicle for the treatment of PCa, and also provide valuable references for all tumors overexpressing folate receptors.

Received 2nd January 2025
Accepted 5th March 2025

DOI: 10.1039/d5na00009b

rsc.li/nanoscale-advances

1. Introduction

Prostate cancer (PCa) is the most common malignancy of the male genitourinary system.[1] The molecular features of PCa include abnormal signaling of the androgen receptor (AR) and phosphatidylinositol 3-kinase (PI3K) pathways.[2] PI3K is a family of intracellular signaling molecules that regulate various signaling pathways, and its overactivation is an important factor in the development and progression of cancers.[3] PI3K is divided into three main classes (Class I, II and III) based on its structure and substrate specificity. Class I/PI3K, the type most associated with human cancers, can be further divided into two main subclasses (Class IA and Class IB).[4] Among the catalytic subunits (p110α, p110β, and p110δ) of Class IA, PI3K/p110β is significantly overexpressed in PCa cells with PTEN dysfunction, and silencing its expression can inhibit AR activity, downregulate the expression of its downstream genes, and inhibit cancer cell proliferation.[5] Therefore, p110β may be an important target for PCa treatment, and its specific inhibitors may become a more effective treatment for advanced castration-resistant PCa.

As the downstream effector of PI3K, the serine and threonine kinase Akt is associated with a variety of diseases including cancers.[6] Studies have shown that PI3K/Akt signaling blocks the expression of pro-apoptotic proteins, reduces tissue apoptosis, and improves the survival rate of cancer cells.[7] The important role of PI3K/110β and the cascaded Akt signaling pathway in the progression of PCa has long been recognized.[8] However, there is still a lack of clinical therapies based on this mechanism.[9]

Endoplasmic reticulum (ER) stress is an important defense mechanism of cells, but persistent or strong ER stress may cause the unfolded protein response (UPR) to activate cell death signals.[10–12] Among the three branches of the UPR, the PERK pathway is the most easily activated.[13] Studies have demonstrated that PERK over activates phosphorylated eIF2a, activates ATF4, and finally activates CHOP, leading to apoptotic death.[14–17] Therefore, drugs that induce excessive ER stress usually exert great antitumor effects. The function of the prostate, an important secretory gland, is mainly dependent on the ER and is therefore susceptible to factors or conditions that cause ER stress.[18] Hence, anti-tumor drugs targeting ER stress are of great clinical significance for PCa treatment.

[a]*Department of Urology, The First Affiliated Hospital of Xi'an Jiaotong University, Xi'an, Shaanxi, 710061, China. E-mail: guopeng661@mail.xjtu.edu.cn*

[b]*Key Laboratory of Natural Medicine and Immune Engineering, School of Pharmacy, Henan University, Kaifeng, Henan, 475004, PR China. E-mail: cenjuan@vip.henu.edu.cn; sduan@henu.edu.cn*

[c]*The First Affiliated Hospital of Henan University, Kaifeng, Henan, 475004, PR China*

[d]*Medical School, Henan University, Kaifeng, 475004, China*

† Electronic supplementary information (ESI) available. See DOI: https://doi.org/10.1039/d5na00009b

‡ W. Xu, X. Li and F. He contributed equally to this paper.

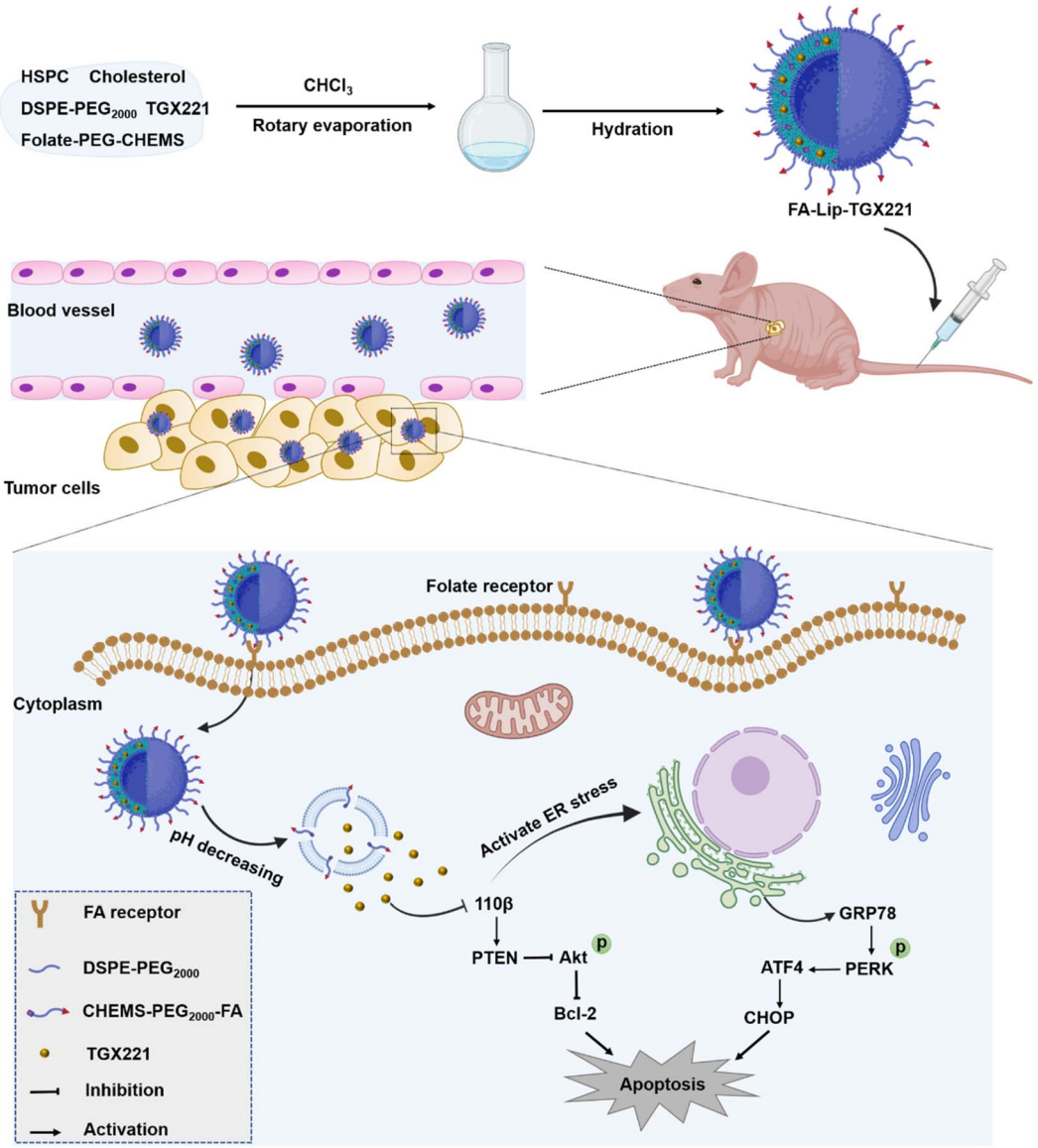

Scheme 1 Illustration of the transport mechanism and inhibitory effect of FA-Lip-TGX221 against prostate cancer.

To date, very few effective specific p110β inhibitors have been reported, among which TGX221 is perhaps the most effective.[19,20] As a synthetic small-molecule inhibitor, TGX221 demonstrates excellent isotype specificity for p110β compared to other types of IA PI3Ks.[21–23] However, its clinical application has been greatly hampered by its poor water solubility.[24]

Due to their low toxicity and ability of encapsulating both hydrophilic and hydrophobic drugs, liposomes have been widely used to improve the therapeutic effect of chemotherapeutic drugs and reduce the side effects.[25–28] For instance, Doxil, prepared by using pegylated liposomes to load doxorubicin, showed a significant inhibitory effect in the treatment of cancers.[29] Notably, extensive studies have demonstrated that liposomes can be modified with various targeting materials to enhance their targeting performance for efficient accumulation of drugs in the focal area.[30]

In this study, we developed a folate receptor-targeted pH-sensitive liposome encapsulating TGX221 (FA-Lip-TGX221) for PCa treatment (Scheme 1). Folate (FA) receptors have been reported to be overexpressed on the surface of many types of cancer cells, including PCa cells.[31] Although quite a few FA-modified liposomes have been reported, FA is always connected to DSPE-PEG to form a targeting material used as a component of the liposomes.[32–34] In our design, FA is connected to cholesterol (Chol) to form FA-PEG-cholesterol semi-succinate (FA-PEG-CHEMS) for the preparation of the targeting liposomes, which has been rarely reported. In addition, almost no research work has been reported on targeted liposomes loaded with TGX-221 in the treatment of PCa. Meanwhile, non-targeted liposomes (Lip-TGX221) without active targeting ability were prepared as the control. The inhibitory effect of FA-Lip-TGX221 on PCa was evaluated *in vitro* and *in vivo*. Experimental results indicated that the ER stress signal of PERK-ATF4-CHOP was significantly

activated by inhibiting the target of PI3K/p110β, thereby ultimately promoting cell apoptosis.

2. Materials and methods

2.1 Materials

Unless otherwise stated, all chemical reagents and organic solvents were purchased from Aladdin Biochemical Technology Co., Ltd (China Limited). Choline 1,2-diacyl-Sn-glycero-3-phosphate (HSPC), cholesterol (Chol) and DSPE-PEG_{2000} were purchased from Avanti (Alabaster, AL, USA). Fluorescent dyes (DAPI, Calcein and DiR) and MTT were purchased from Beyotime Biotechnology Co., Ltd (China). Fetal bovine serum (FBS), F12K culture-medium, trypsin EDTA, 1% penicillin and streptomycin were purchased from GIBCO-BRL (Grand Island, NY, USA). All reagent test kits for cell experiments and all reagents for western blotting were purchased from Beyotime Biotechnology Co., Ltd (China). All biochemical reagents were used without further purification.

2.2 Preparation of FA-PEG-CHEMS

To prepare FA-PEG-CHEMS, the EDC/NHS coupling method was used. In brief, FA (26.5 mg), DCC (15.5 mg), NHS (8.63 mg) and TEA (48 μL) were dissolved in DMSO to form a homogeneous solution, followed by the addition of H_2N-PEG-NH_2 (167.5 mg). After the reaction was continued at room temperature in the dark for 1 h, 50 mM Na_2CO_3 was added and the solution was centrifuged. The final product was purified by using a Sephadex G25 column and lyophilized to obtain FA-PEG-bis-amine. Next, CHEMS (1 g), NHS (0.475 g) and DCC (1.25 g) were dissolved in THF and reacted overnight at room temperature in the dark. After the reaction, the product was purified by the recrystallization method, and the final product was vacuum dried to obtain EMS-NHS. Finally, FA-PEG-bis-amine (137 mg) and CHEMS-NHS (29.2 mg) were dissolved in $CHCl_3$ and reacted overnight at room temperature in the dark. The unreacted residues were removed through dialysis in ddH_2O for 2 days (MWCO: 14 KDa) and lyophilization was performed to afford the desired FA-PEG-CHEMS.

2.3 ^{1}H NMR and FT-IR spectra

Proton nuclear magnetic resonance (^{1}H NMR) spectra were recorded using a nuclear magnetic resonance spectrometer (500 MHz, Bruker, Switzerland) and FT-IR spectra were measured by the KBr particle method and recorded on a Bruker IFS-55 (Switzerland).

2.4 Preparation of liposomes

Folate-targeting liposomes (FA-Lip-TGX221) were prepared by the thin film hydration method. The mass ratio of HSPC, Chol, DSPE-$mPEG_{2000}$ and FA-PEG-CHEMS was 64 : 4 : 9 : 6. Then, liposomes and TGX221 (lipid-to-drug mass ratio 10 : 1) were dissolved in trichloromethane. The organic solvent was then removed by vacuum evaporation at 37 °C until a lipid film was formed on the inner wall of the round-bottomed flask. At room temperature, the flask was placed in a vacuum drying oven overnight to remove residual organic solvents. Next, the film was hydrated with PBS at 65 °C for 30 min, and the obtained liposome suspension was extruded three times through a 220 nm polycarbonate membrane. Finally, the free TGX221 was separated from the liposome by using a Sephadex G25 gel column. For the preparation of non-folate targeted liposomes (Lip-TGX221), HSPC, Chol, and DSPE-$mPEG_{2000}$ were mixed at a mass ratio of 64 : 13 : 6, and other operations were carried out as described above. Liposomes containing Calcein (green fluorescence) and DiR (red fluorescence) were prepared for the determination of cellular uptake and distribution of liposomes *in vivo*, respectively. Calcein-loaded liposomes (Lip-Calcein) and DiR-loaded liposomes (Lip-DiR) were prepared by replacing TGX221 with Calcein and DiR, respectively.

2.5 Characterization of liposomes

The size and zeta potential of the liposomes were measured at 25 °C using a Zetasizer Nano ZS90 (Malvern, UK). The morphology of liposomes was observed by transmission electron microscopy (JEM-2100 Plus, JEOL, Japan). The absorption spectrum of TGX221 was obtained by using a UV-vis spectrophotometer (RF-5301 PC, Shimadzu, Kyoto, Japan). The encapsulation rate (EE%) and drug loading (DL%) of TGX221 were determined by using the ultraviolet spectrum (280 nm). The calculation formula is as follows:

$$\mathrm{DL}\% = \text{weight of TGX221 in lips/weight of lips}$$

$$\mathrm{EE}\% = \text{weight of TGX221 in lips/weight of feeding lips}$$

2.6 *In vitro* stability and drug release

To test the stability of liposomes, Lip-TGX221 and FA-Lip-TGX221 were incubated with H_2O and 10% FBS, respectively. All samples were stored at 4 °C and the size and potential changes in the liposomes were measured for a predetermined period of time (n = 3 per group). The release of liposomes *in vitro* was studied by the dialysis method. Briefly, TGX221 and Lip-TGX221 were transferred into dialysis bags (MWCO: 1000 Da) and then dialyzed in PBS at pH 7.4, while FA-Lip-TGX221 was dialyzed in PBS with different pH values. The whole process was conducted at 150 rpm and 37 °C for 96 h. At each predetermined time point, three equal samples were withdrawn and the cumulative amount of TGX221 released was measured at 280 nm using a UV-vis spectrophotometer (RF-5301 PC, Shimadzu, Kyoto, Japan).

2.7 Cell lines and animals

A human prostate cancer cell line (PC-3) was purchased from China Scientific Cell Bank (Shanghai, China). PC-3 cells were cultured in F12K medium containing 10% fetal bovine serum (FBS), 100 μg per mL streptomycin and 100 U per ml penicillin in a cell incubator (37 °C, 5% CO_2).

Male BALB/c nude mice (weight: 15–19 g) were purchased from the Henan Experimental Animal Center (Zhengzhou, China). All *in vivo* antitumor studies were performed in accordance with the National Research Council's Guide for the Care

and Use of Laboratory Animals, and approved by the Animal Experiment Ethics Committee of Henan University (Approval number: HUSOM2020-147).

2.8 *In vitro* cell uptake studies

In order to observe the cellular uptake behavior of the liposomes, Calcein was selected as a fluorescent dye to label the liposomes. Briefly, PC-3 cells were inoculated into 6-well plates at a density of 5×10^5 per well and cultured for 24 h, followed by incubation with free Calcein, Lip-Calcein, FA-Lip-Calcein or FA (1 mM) + FA-Lip-Calcein (15 μM) for 6 h, respectively. Finally, the cells were washed with PBS, fixed with 4% paraformaldehyde, and treated with DAPI (0.1 μg mL^{-1}) for nuclear staining. Imaging was performed using an Olympus BX43 CKX31, and the cellular uptake efficiency was investigated by flow cytometry (Cyto FLEX, Beckman).

2.9 *In vitro* endocytosis pathway study

The effects of various inhibitors on cellular uptake of liposomes were investigated using PC-3 cells. Briefly, PC-3 cells were inoculated into 6-well plates at a density of 5×10^5 per well and cultured for 24 h, followed by pre-incubation at 37 °C for 30 min with various inhibitors, such as colchicine, amiloride, chlorpromazine, methyl-beta-cyclodextrin and broxanthine. Then, the medium containing inhibitors was discarded and a fresh medium containing Calcein-labeled liposomes was added for 6 h of incubation. Finally, the cells were treated and fluorescence intensity was detected by FCM.

2.10 *In vitro* cytotoxicity studies

MTT assay was used to evaluate the cytotoxicity of drugs at different concentrations. Briefly, PC-3 cells were inoculated into 96-well plates at a density of 8×10^3 per well and cultured at 37 °C for 24 h. Then, the cells were treated with TGX221, Lip-TG221, and FA-Lip-TGX221 at varying concentrations of 2.5 to 80 μg mL^{-1} and cultured at 37 °C for 24, 48, and 72 h, respectively. Next, MTT (10 μL, 0.5 mg mL^{-1}) was added to each well and incubated for 4 h, followed by the removal of the medium and addition of DMSO (100 μL). The absorbance was measured at 490 nm using a microplate reader (Multiscan, Thermo, USA).

The viability of live and dead cells was used for qualitative study of cytotoxicity. PC-3 cells were inoculated into six-well plates at a density of 5×10^5 per well and incubated with TGX221, Lip-TG221, and FA-Lip-TGX221 for 24 h. Calcein-AM was added at 37 °C for 30 min and propyl iodide (PI) for 2–5 min. The cells were then observed under a fluorescence inverted microscope.

2.11 EdU cell proliferation experiment

PC-3 cells were inoculated into 96-well plates at a density of 8×10^3 cells per well, followed by incubation at 37 °C for 24 h. After 24 h of drug treatment, cells were incubated with 10 μM EdU for 2 h and then cultured for 24 h. The cells were then fixed with 4% paraformaldehyde for 30 min and incubated with 0.5% Triton X-100 PBS solution at room temperature for 20 min. Next, 100 μL Apollo solution was added to each well, followed by incubation in the dark for 30 min. Finally, fluorescence imaging was performed under a fluorescence microscope. ImageJ was used for statistics and the cell proliferation rate was calculated.

2.12 Tunnel assay

PC-3 cells were inoculated into 96-well plates at a density of 8×10^3 cells per well. After the cells were attached to the wall and treated with drugs for 24 h, they were fixed in 4% paraformaldehyde for 30 min and incubated at room temperature for 5 min with cell permeable solution. A TUNEL test solution was prepared according to the instructions, and then 50 μL was added to each well, followed by incubation for 60 min in the dark. DAPI was used for nuclear staining at room temperature in the dark. Finally, fluorescence imaging was conducted under a fluorescence inverted microscope. ImageJ was used for statistics and the cell apoptosis rate was calculated.

2.13 Cell apoptosis and cycle experiment

PC-3 cells were inoculated in 6-well plates at a density of 5×10^5 cells per well and incubated with TGX221, Lip-TG221, and FA-Lip-TGX221 for 24 h, respectively. Staining was performed with the YF®488 Annexin V and PI apoptosis assay kit or cell cycle kit, and then apoptotic cells and cell cycle were detected by flow cytometry (FCM) and analyzed employing FlowJo software.

2.14 Mitochondrial membrane potential (MMP) detection

A JC-1 kit was used to detect MMP in PC-3 cells. PC-3 cells were inoculated in six-well plates at a density of 5×10^5 cells per well and incubated with TGX221, Lip-TG221, and FA-Lip-TGX221 for 24 h. According to the kit instructions, JC-1 staining was performed on the cells, with CCCP+ as the positive control group. Finally, the cells were imaged under a fluorescence inverted microscope.

2.15 Western blot

Proteins were extracted from cells or tumor tissues, separated in a 10% SDS polyacrylamide gel, transferred to a 0.45 μm PVDF membrane and then sealed with a sealer solution at room temperature. After that, they were incubated at 4 °C overnight with anti-p110β, anti-GRP78, anti-Bcl-2, anti-Akt, anti-p-Akt, anti-p-PERK, anti-PTEN, anti-ATF4, anti-CHOP, and anti-GAPDH antibodies, respectively. A PVDF membrane was incubated with Goat anti-Rabbit IgG (H + L) HRP at room temperature for 1 h. Protein expression was quantified using ImageJ software.

2.16 *In vivo* imaging analysis

In order to explore the targeting effect of folate-targeted liposomes on prostate cancer, we prepared BALB/c mice with prostate cancer by subcutaneous injection of approximately 2×10^6 PC-3 cells in the right axillary area. The mice were divided into three groups (DiR, Lip-DiR and FA-Lip-DiR) , with three mice in each group. When the tumor volume reached 200 mm^3, 100 μL of DiR formulation (equivalent to 0.2 mg per kg DiR) was administered through the caudal vein. Mice were photographed at 1, 3, 6, 12, 24, and 48 h using a small animal optical imaging system (IVIS Lumina XRMS Series III, USA) with an excitation wavelength of

748 nm and emission wavelength of 780 nm. After 48 h, the mice were sacrificed, and the tumors and major organs were collected for *in vitro* fluorescence imaging.

2.17 *In vivo* antitumor studies

The subcutaneous PC-3 tumor bearing mouse model was established to evaluate the therapeutic effect of different drug preparations. In brief, each mouse was inoculated with 2×10^6 PC-3 cells. When the tumor grew up to 100 mm^3, the mice were randomly divided into 4 treatment groups ($n = 7$), which were the control group (normal saline), free TGX221, Lip-TGX221, and FA-Lip-TGX221. The dose of TGX221 was 100 mg kg^{-1}. The drug was administered through the caudal vein every other day for 14 days. The diameter and weight of the tumor were measured every other day, and the tumor length (a) and width (b) were measured with vernier calipers. Tumor volume was calculated according to the following formula: tumor volume (mm^3) = $(a \times b^2)/2$ at the end of the experiment. The mice were killed and blood samples from each group were collected for biochemical analysis. In addition, tumors and major organs (heart, lung, liver, spleen, and kidney) were collected and H&E staining was performed to assess the pathological changes in tumors and major organs. Immunohistochemical staining of proliferative markers, including Ki-67, was performed to assess tumor proliferation in each group. Apoptosis of tumor tissue was observed by the TUNEL method.

2.18 Data analysis

All data in this study were expressed as mean ± standard deviation (SD). With GraphPad Prism 9.0 software, univariate analysis of variance (ANOVA) was used to analyze the differences between the groups. $^*P < 0.05$ was considered statistically significant; $^{**}P < 0.01$, $^{***}P < 0.001$ and $^{****}P < 0.0001$ are very significant; NSD, no significant difference, $P > 0.05$.

3. Results and discussion

3.1 Preparation and characterization of FA-PEG-CHEMS

FA-PEG-CHEMS was successfully prepared according to the synthetic route (Fig. 1A). The successful preparation of FA-PEG-CHEMS was confirmed by ^{1}H NMR and FTIR spectra.

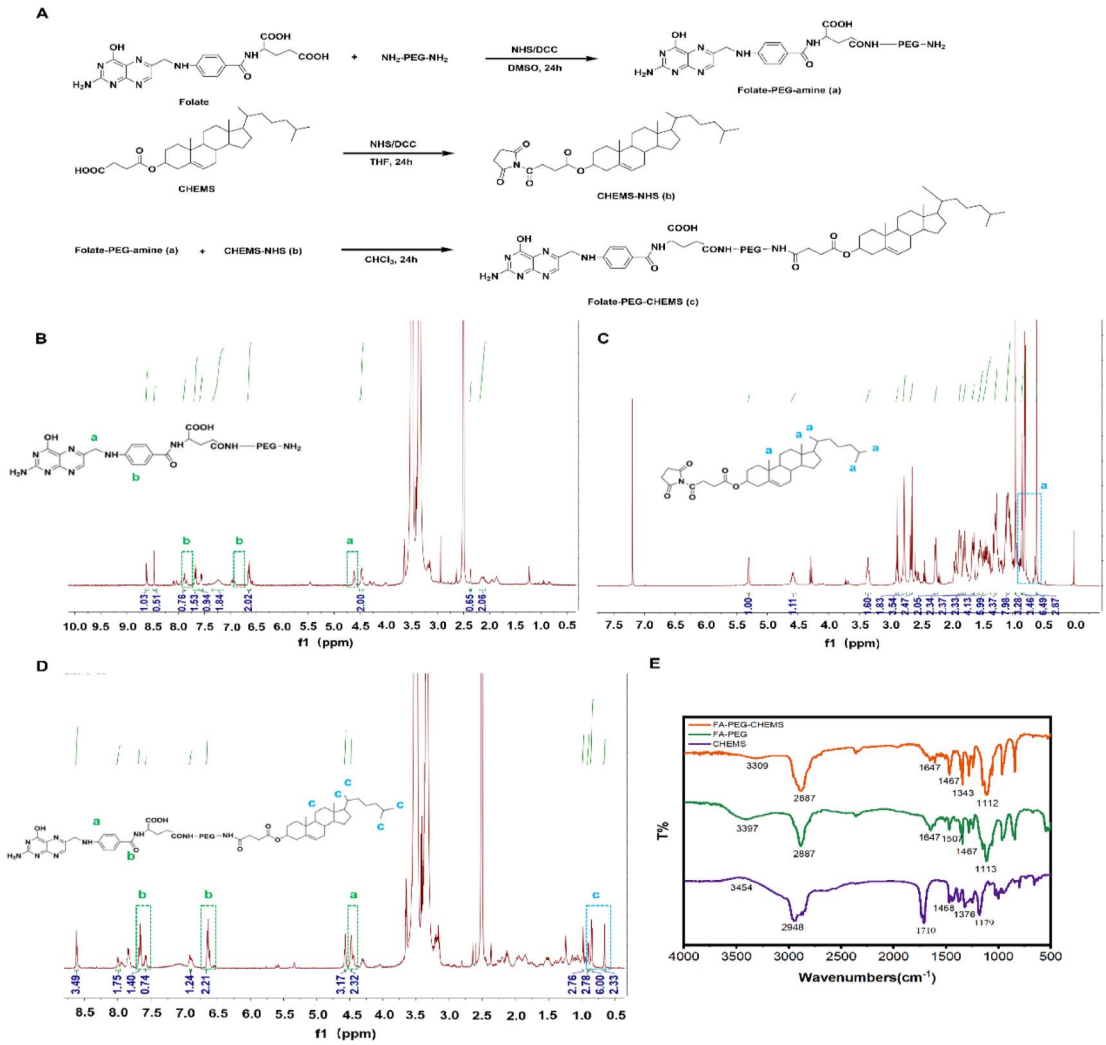

Fig. 1 (A) Synthesis of FA-PEG-CHEMS. ^{1}H NMR spectra of (B) FA-PEG-bis-amine (DMSO-d_6, 500 MHz), (C) CHEMS-NHS, ($CDCl_3$-d_6, 500 MHz), and (D) FA-PEG-CHEMS (DMSO-d_6, 500 MHz). (E) FT-IR spectra of FA-PEG-bis-amine, Chaves-NHS and FA-PEG-CHEMS.

As shown in Fig. 1B–D, ^{1}H NMR spectra show that signals at 4.3–4.5 ppm (methylene proton) and 6.6–6.7 ppm and 7.6–7.7 ppm (benzene ring) belong to the characteristic peaks of FA. The characteristic peak at 0.58–0.98 ppm belongs to the methyl proton on CHEMS. From the FT-IR spectrum of FA-PEG-CHEMS shown in Fig. 1E, it can be observed that the absorption peak at 3309 cm^{-1} is N–H stretching vibration absorption of the amide bond. The absorption peak at 2887 cm^{-1} is due to the symmetric stretching characteristic of methyl–methyl of CHEMS, and the absorption peak at 1343 cm^{-1} was CH_3. The peak at 1647 cm^{-1} is the C=O stretching vibration absorption peak of the amide bond. The characteristic absorption peak of the benzene ring in FA was at 1467 cm^{-1}. The absorption peak at 1112 cm^{-1} is the stretching vibration absorption peak of C–O–C of H_2N-PEG-NH_2. Therefore, these ^{1}H NMR spectra and FT-IR spectra demonstrate the successful synthesis of FA-PEG-CHEMS.

3.2 Preparation and characterization of FA-Lip-TGX221

In this study, we used liposomes as the drug carrier for the targeted delivery of TGX221 to PCa cells. As shown in Fig. 2A, the liposomes were prepared using the thin film water method.

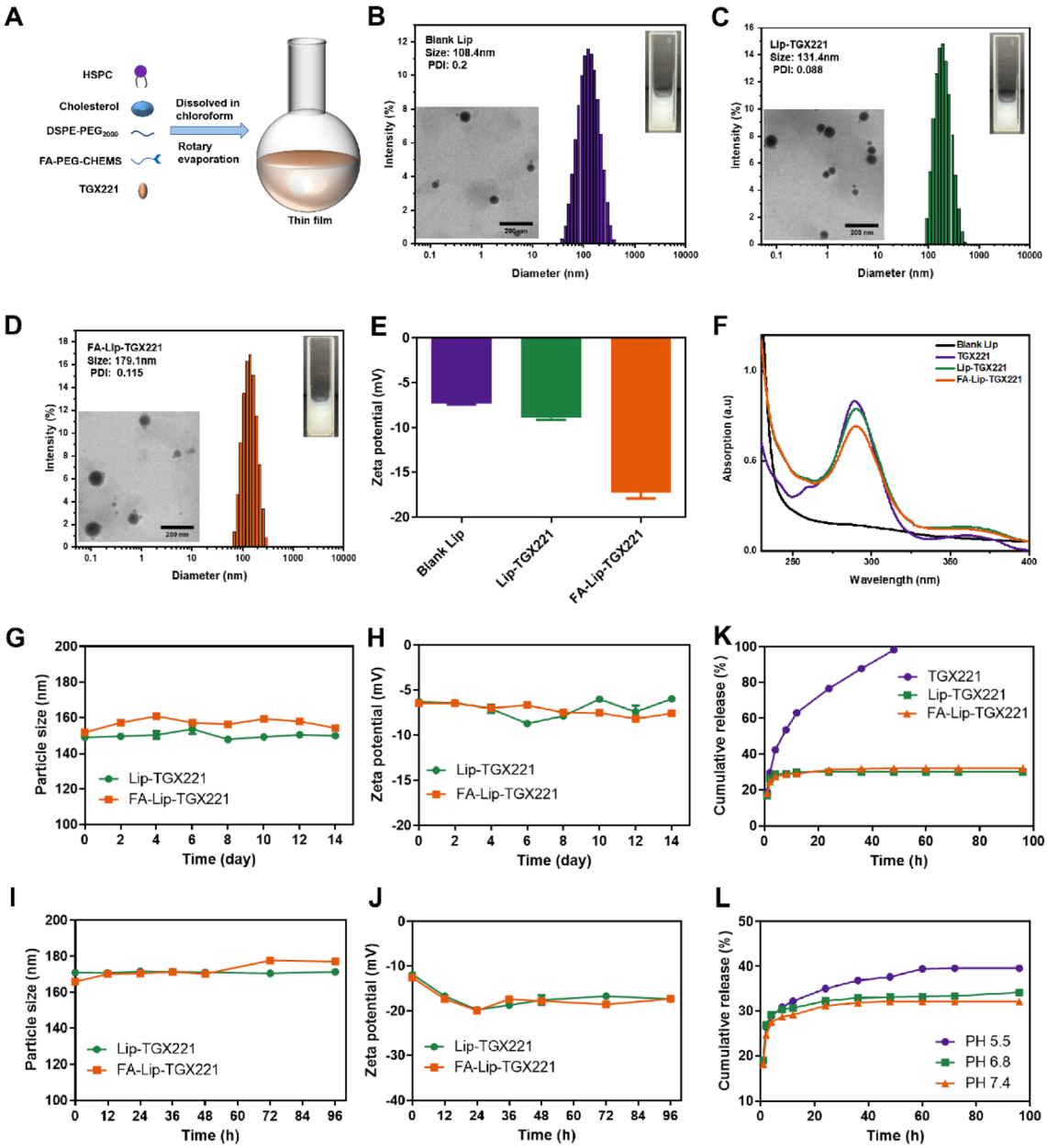

Fig. 2 Characterization of liposomes. (A) Schematic diagram of liposome synthesis. (B–D) the particle size distribution and transmission electron microscopy of Blank-Lip, Lip-TGX221 and FA-Lip-TGX221, respectively [scale = 200 μm]. (E) Zeta potential statistics. (F) UV spectrum. Particle size and potential stability of (G and H) liposomes at 4 °C. (I and J) Particle size and potential stability of liposomes in 10% FBS. (K) Cumulative drug release curves of TGX221, Lip-TGX221, and FA-Lip-TGX221 in buffers at pH 7.4. (L) Cumulative release curves of FA-Lip-TGX221 in buffers with different pH values (pH = 5.5, 6.8, 7.4) (mean ± SD, n = 3).

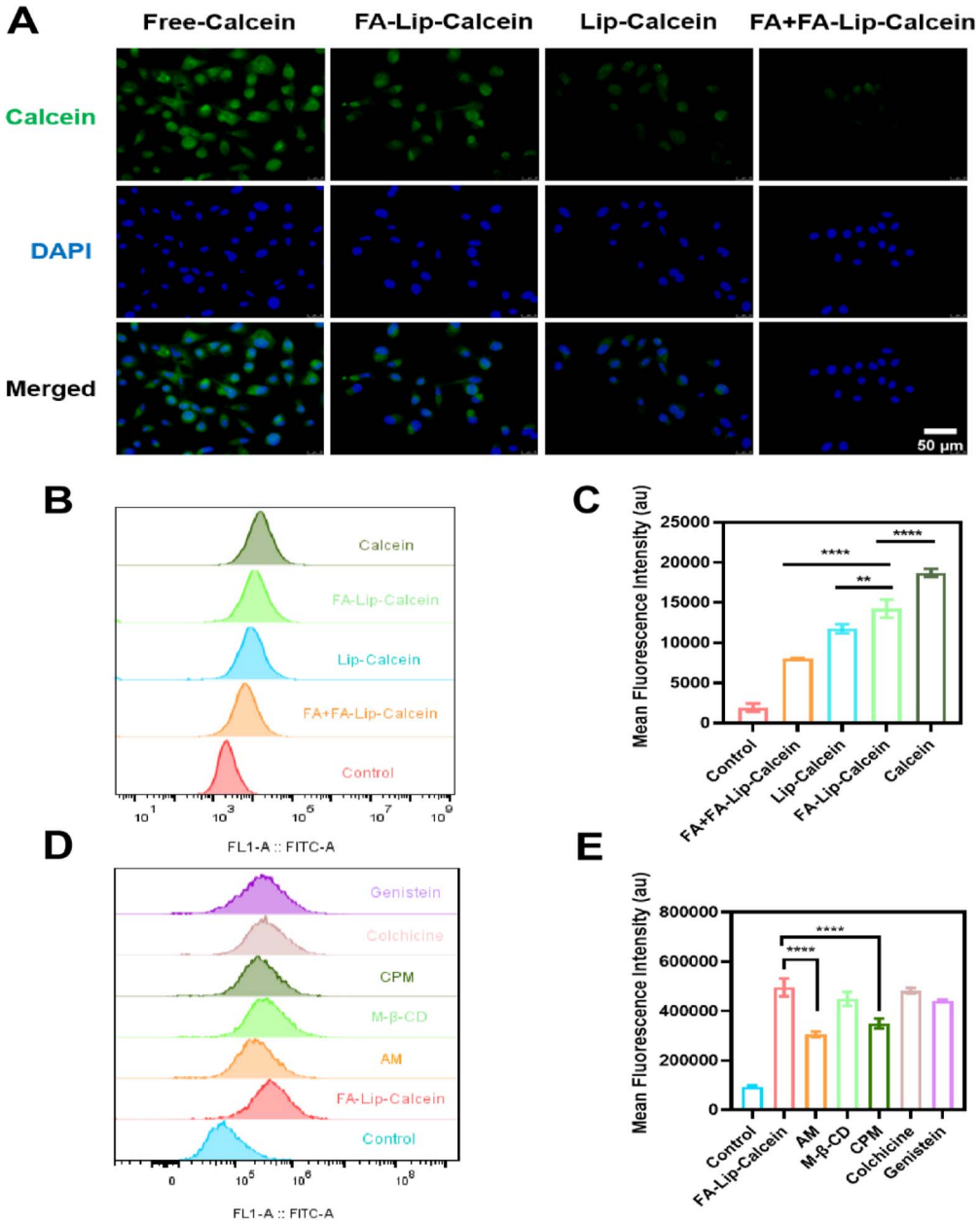

Fig. 3 *In vitro* cellular uptake of liposomes. (A) Fluorescence microscopy images of PC-3 cells after incubation with free Calcein, Lip-Calcein, and FA-Lip-Calcein for 6 h, in which the nuclei were labeled with DAPI (blue) and the Lip with Calcein (green) [scale = 50 μm]. (B) FCM image of Calcein fluorescence intensity. (C) Calcein fluorescence intensity was quantitatively determined by flow cytometry. (D) FCM images of PC-3 cells after incubation with different inhibitors. (E) Calcein fluorescence intensity was quantitatively determined by flow cytometry (mean ± SD, $n = 3$, $^{**}P < 0.01$ or $^{****}P < 0.0001$).

Table 1 Physical and chemical properties of different liposomes (25 °C). Mean ± SD ($n = 3$)

Sample	Size (nm)	PDI	Zeta (mV)	EE (%)	DL (%)
Blank Lip	106.79 ± 6.76	0.206 ± 0.01	−7.31 ± 0.20	—	—
Lip-TGX221	130.10 ± 1.54	0.064 ± 0.02	−8.89 ± 0.39	81.13 ± 1.19	5.80 ± 0.09
FA-Lip-TGX221	186.10 ± 8.03	0.165 ± 0.55	−17.27 ± 1.10	79.97 ± 5.11	5.71 ± 0.37

Then, TGX221 was encapsulated into the hydrophobic layer of the liposomes. As shown in Fig. 2B–D, the liposomes, including Blank Lip, Lip-TGX221, and FA-Lip-TGX221, demonstrated uniform spheres, and their average particle sizes ranged from 108 to 180 nm with a narrow size distribution (PDI < 0.20). Meanwhile, their zeta potentials were −7.31 ± 0.20 mV, −8.89 ±

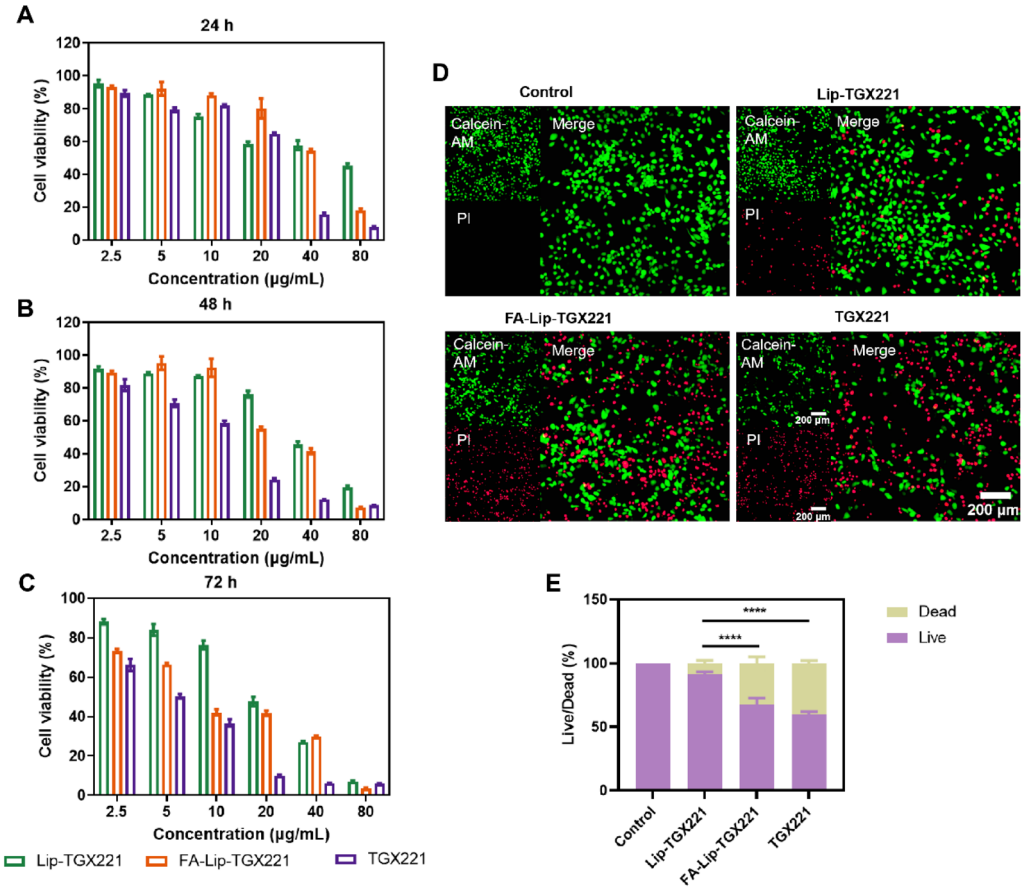

Fig. 4 Cytotoxicity of different drug formulations. Cytotoxicity of free TGX221, Lip-TGX221, and FA-Lip-TGX221 to PC-3 cells at (A) 24 h, (B) 48 h, and (C) 72 h. (D) Live/dead staining of PC-3 cells, where cells stained green and red represent live and dead ones, respectively [scale = 200 μm]. (E) ImageJ was utilized to determine fluorescence intensity quantitatively (mean ± SD, $n = 3$, ****$P < 0.0001$).

0.39 mV, and −17.27 ± 1.10 mV, respectively (Fig. 2E). In addition, the typical absorption peak of TGX221 (280 nm) was observed in the full-wavelength UV scanning of Lip-TGX221 and FA-Lip-TGX221, confirming that TGX221 was well encapsulated into the liposomes (Fig. 2F). The drug loading (DL) and encapsulation efficiency (EE) of the liposomes were calculated by using a UV-vis spectrophotometer. As shown in Table 1, the DL of Lip-TGX221 and FA-Lip-TGX221 was 5.80 ± 0.09% and 5.71 ± 0.37%, respectively, and the EE was 81.13 ± 1.19% and 79.97 ± 5.11% respectively.

In order to evaluate the stability of the drug-loaded liposomes, we placed them in various environments and then detected the changes in their particle sizes and potentials. We found that after long-term storage in PBS at 4 °C (Fig. 2G–H) and a simulated physiological environment in 10% FBS (Fig. 2I and J), the sizes and zeta potentials of the liposomes did not change significantly, suggesting their good physiological stability.

The release behavior of TGX221 from liposomes was evaluated in buffers at different pH values (7.4, 6.8, and 5.5) by the dialysis method, among which pH 7.4 represented the normal physiological environment, while pH 6.8 and pH 5.5 were chosen to simulate an acidic tumor microenvironment. First, *in vitro* release of free TGX221, Lip-TGX221, and FA-Lip-TGX221 was detected in PBS buffers containing Tween 80 (5%) (pH 7.4). The release of free TGX221 was almost complete at 48 h, whereas the cumulative drug release of Lip-TGX221 and FA-Lip-TGX221 was only about 30%, indicating that the liposomes retained most of the loaded drugs under normal physiological conditions (Fig. 2K), which indirectly proved the excellent stability of the liposomes. CHEMS contains ester bonds that become unstable under acidic conditions.[33] To demonstrate that the release curve of FA-Lip-TGX221 was pH-dependent, they were incubated in PBS buffers with different pH values. The results showed that the release rate of TGX221 from FA-Lip-TGX221 increased as the buffer pH decreased. In particular, the cumulative percentage of TGX221 released from FA-Lip-TGX221 in the acid buffer (pH 5.5) reached approximately 40% after 60 h of incubation, which was significantly higher than that at pH 7.4. In addition, it was also shown that drug release leveled off after 60 h. Therefore, folate-targeted liposomes based on CHEMS released the drug more easily in an acidic tumor microenvironment, and the drug was released in a sustained release manner.

3.3 Determination of cellular uptake and endocytosis pathways *in vitro*

The cellular uptake efficiency of various liposomes was observed by fluorescence microscopy and FCM employing Calcein (Green fluorescence) as the fluorescent probe. As shown in Fig. 3A, different drug administration groups showed different intensities of green fluorescence after co-incubation with PC-3 cells. Specifically, the fluorescence intensity of Calcein in the FA-Lip-Calcein group was 1.36 times stronger than that of the Lip-Calcein group. In order to verify folate receptor-mediated endocytosis, we added excess free FA to block the folate receptors on PC-3 cells prior to incubation with FA-Lip-Calcein. It was shown that the fluorescence intensity of the FA + FA-Lip-Calcein group was significantly lower than that of the FA-Lip-Calcein group, indicating that the specific binding of FA to the folate receptor could improve the uptake efficiency of liposomes. In addition, fluorescence imaging was utilized to investigate the targeting ability of FA. As shown in Fig. 3B and C, the cellular uptake results quantified by FCM were consistent with those in Fig. 3A. All these results suggested that the folate receptor-mediated endocytosis pathway significantly increased intracellular delivery of liposomes.

Next, FCM was utilized to evaluate the inhibitory effect of various inhibitors on the uptake of FA-Lip-Calcein by PC-3 cells, so as to further study the cellular uptake mechanism. Herein, the inhibitors we utilized included microtubule formation and macropinocytosis inhibitor colchicine, lipid raft inhibitor methyl-β-cyclodextrin (M-β-CD), fossa endocytosis related tyrosine kinase inhibitor genistein (genistein), clathrin-mediated endocytosis inhibitor chlorpromazine (CPZ), and pinocytosis inhibitor amiloride (AM).[34,35] As shown in Fig. 3D and E, after the cells were preincubated with the inhibitors, the intracellular

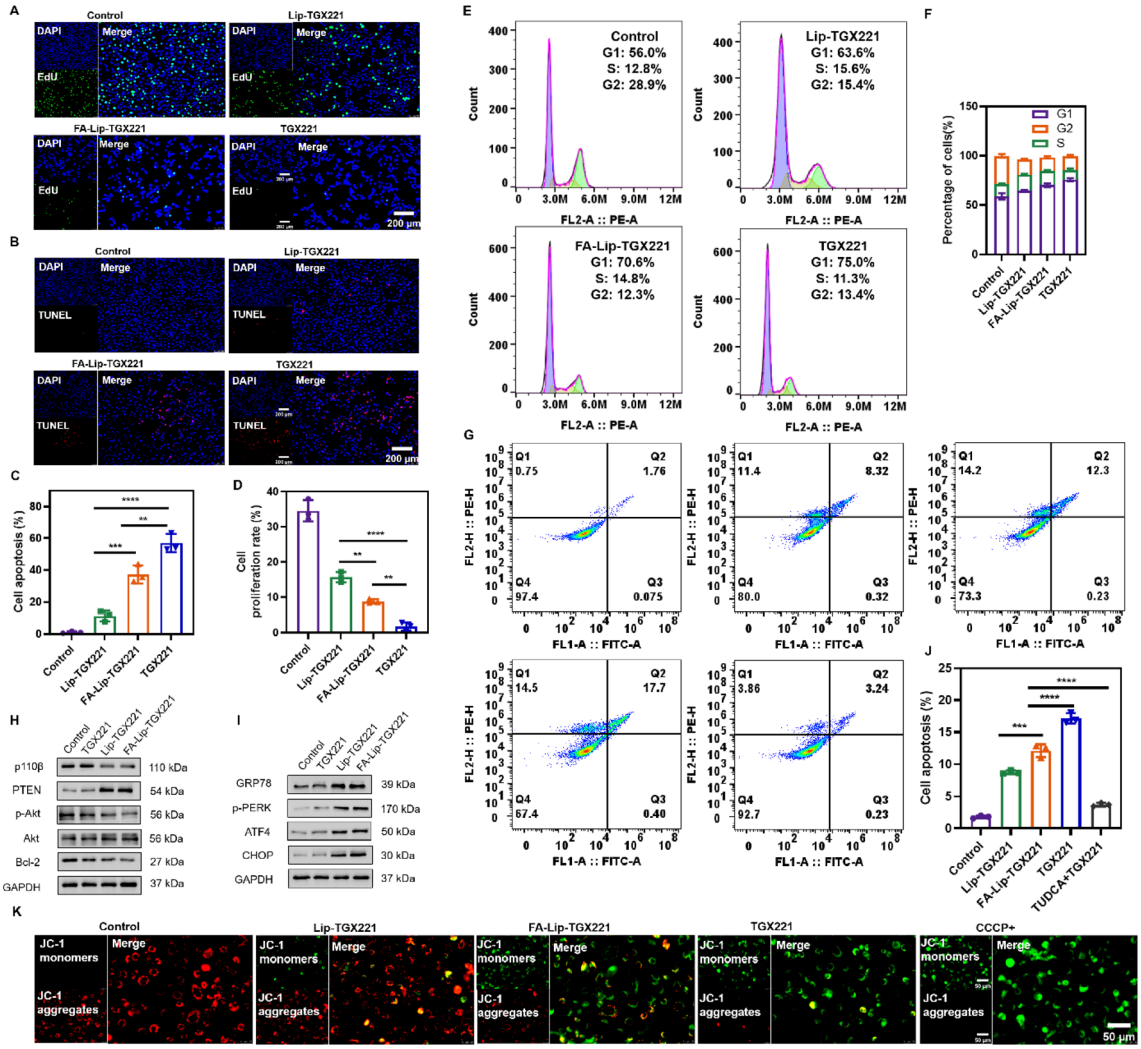

Fig. 5 (A) DNA replication activity of PC-3 cells in each group was detected by the EdU method [scale = 200 μm]. (B) Cell apoptosis was determined by the TUNEL method [scale = 200 μm]. (C) Cell proliferation rate in each group was analyzed. (D) Calculation formula of the apoptosis index: apoptosis index = (apoptotic cells with positive staining)/(total number of cells) × 100%. (E) The cell cycle distribution of PC-3 cells was determined by flow cytometry. (F) Statistical analysis of cell cycle outcomes. (G) Flow cytometry was used to detect the apoptosis rate of PC-3 cells in different preparation groups. (H) Quantitative analysis of proteins associated with the PI3K/Akt signaling pathway. (I) Quantitative analysis of ER stress-related proteins. (J) The percentage of apoptotic cells (%) was calculated. (K) Fluorescence images of mitochondrial membrane potential detected by the JC-1 method [scale = 50 μm] (mean ± SD, $n = 3$, $^{**}P < 0.01$, $^{***}P < 0.001$ or $^{****}P < 0.0001$).

fluorescence intensity of the CPZ inhibitor group and the AM inhibitor group significantly decreased compared with that of the FA-Lip-Calcein group, suggesting that the liposomes were taken up by cells mainly through clathrin-mediated endocytosis and micropinocytosis.

3.4 *In vitro* cytotoxicity test

In vitro cytotoxicity of different drug formulations to PC-3 cells was evaluated by MTT assay. As shown in Fig. 4A–C, concentration- and time-dependent cytotoxicity was observed in all the drug treatment groups, among which FA-Lip-TGX221 showed higher cytotoxicity than Lip-TGX221. Notably, the IC_{50} value of the non-targeted Lip-TGX221 group was 19.06 μg mL^{-1} for 72 h, while that of FA-Lip-TGX221 was 9.60 μg mL^{-1}, implying that the inhibitory effect of the folate-targeted liposomes on cell proliferation was about 2 times that of the non-targeted liposomes, confirming that the folate-targeted liposomes had stronger cell-killing ability.

In this study, living/dead cells were stained with green (Calcein-AM) and red (PI) fluorescent dyes respectively for activity determination. As shown in Fig. 4D and E, there were more red fluorescence signals in the FA-Lip-TGX221 group than in the LiP-TGX221 group, further indicating that the targeted therapy based on the folate-targeted liposomes exhibited excellent cytotoxicity.

3.5 *In vitro* cell proliferation and apoptosis tests

The proliferative effect of FA-Lip-TGX221 on PC-3 cells was evaluated by EdU assay. As shown in Fig. 5A–C, the cell proliferation rates of PC-3 cells in the FA-Lip-TGX221 group and Lip-TGX221 group were 8.80 ± 0.55% and 15.70 ± 1.19%, respectively, under the same treatment condition as Calcein-AM/PI staining. According to the TUNEL results in Fig. 5B–D, the apoptosis index of the FA-Lip-TGX221 group was significantly higher than that of the Lip-TGX221 group. Quantitative analysis showed that the apoptosis rate of PC-3 cells in the FA-Lip-TGX221 group was 37.30 ± 4.58%, which was significantly higher than that in the Lip-TGX221 group (11.28 ± 2.70%).

Accordingly, the cell cycle analysis results showed that compared with the control group, the cell cycle in the FA-Lip-TGX221 group was mainly blocked in the G1 phase, which is the early stage of DNA synthesis, resulting in the obstruction of DNA synthesis in tumor cells, thereby inhibiting the proliferation of tumor cells (Fig. 5E and F).

In order to further investigate the apoptosis effect of FA-Lip-TGX221 on PC-3 cells, we employed Annexin V-FITC/PI assay to perform apoptosis experiments by FCM. As shown in Fig. 5G–J, the mean apoptosis rates of the control group, TGX221 group, Lip-TGX221 group and FA-Lip-TGX221 group were 1.81%, 17.18%, 8.76% and 12.11%, respectively. Notably, compared with the Lip-TGX221 group, both early and late apoptotic cells in the FA-Lip-TGX221 group increased.

In addition, mitochondrial membrane potential (MMP) was detected by JC-1 staining to detect the early stages of apoptosis. When MMP is reduced, the JC-1 aggregates (red light) in mitochondria are transformed into JC-1 monomers (green light). Therefore, MMP reduction is a landmark event in the early stage of apoptosis. After MMP was reduced by CCCP+ treatment (positive control), JC-1 did not retain its polymer form in the mitochondrial matrix, resulting in a significant decrease in mitochondria with red fluorescence and an increase in

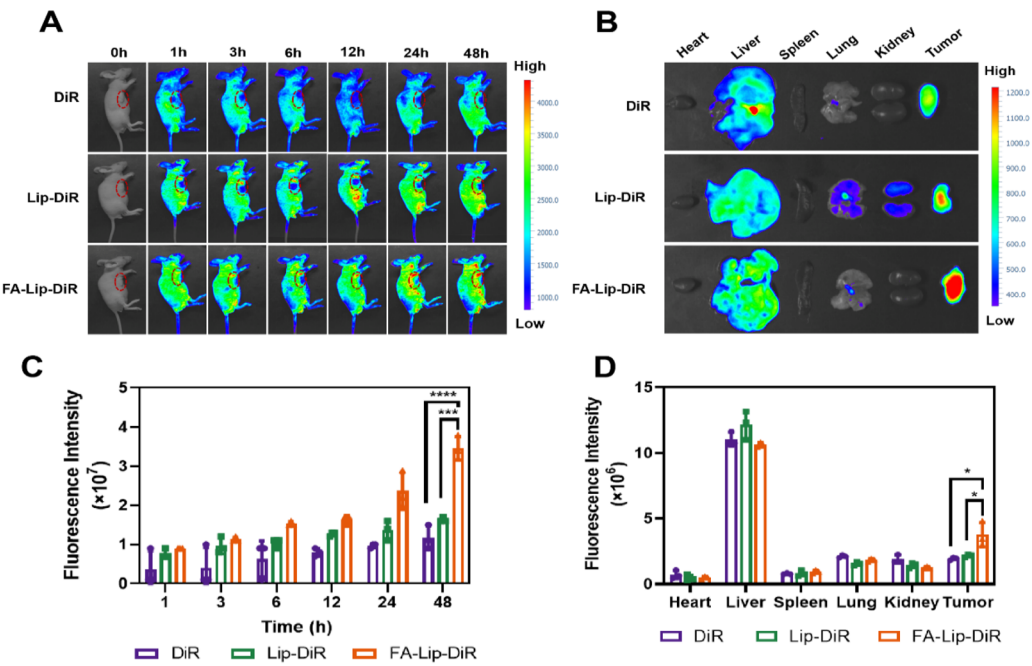

Fig. 6 Biological distribution *in vivo*. (A) Whole body images at different time points after the administration of free DiR, Lip-DiR, or FA-Lip-DiR *via* the caudal vein ($n = 3$) at a dose of 0.5 mg per kg DiR. (B) Images of major tissues obtained at 48 h post injection. (C) Quantitative analysis of fluorescence intensity in tumor regions at different time points. (D) Quantitative analysis of fluorescence intensity in major organs and tumor tissues (mean ± SD, $n = 3$, *$P < 0.05$, ***$P < 0.001$ or ****$P < 0.0001$).

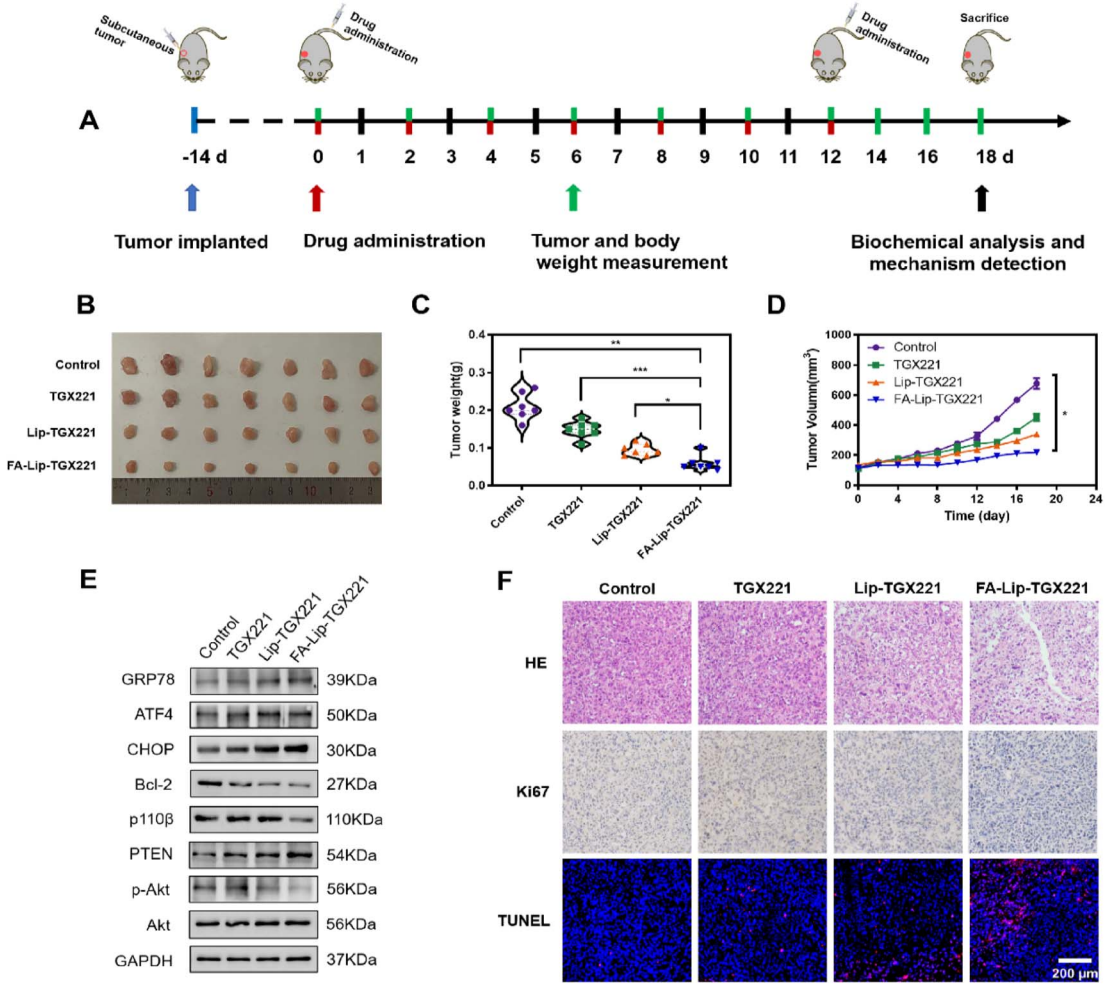

Fig. 7 Antitumor effect of TGX221 liposomes *in vivo*. Free TGX221, Lip-TGX221, FA-Lip-TGX221 and the same volume of normal saline were injected every 2 days at 100 mg kg^{-1} TGX221 through the caudal vein. (A) Timeline from inoculation of PC-3 cells to the end of treatment. (B) Images of tumor resection after various treatments. (C) The weight of the tumor removed after various treatments. (D) The change curve of tumor volume in mice after different treatments. (E) Changes in the expression levels of the PI3K/Akt signaling pathway and ER stress-related proteins. (F) H&E staining, Ki-67 staining and TUNEL staining of tumor sections in different treatment groups [scale = 200 μm] (mean ± SD, $n = 7$, $^{*}P < 0.05$, $^{**}P < 0.01$ or $^{***}P < 0.001$).

cytoplasm with green fluorescence. As shown in Fig. 5K, PC-3 cells incubated with FA-Lip-TGX221 showed brighter green fluorescence from JC-1 monomer staining, and the fluorescence intensity was significantly higher than that of Lip-TGX221. These results indicate that FA-Lip-TGX221 could effectively induce a decrease in MMP in PC-3 cells and promote the apoptosis of PC-3 cells.

Next, western blot was performed o detect the expression level of the target proteins in PC-3 cells after treatment with FA-Lip-TGX221. As shown in Fig. 5H, the expression of 110β was decreased, the expression of PTEN was increased, the phosphorylation level of Akt was decreased, and the expression of anti-apoptotic factor Bcl-2 was decreased. These results suggested that FA-Lip-TGX221 further promoted the apoptosis of PC-3 cells and inhibited proliferation of PC-3 cells by down-regulating the activation of the PI3K/Akt signaling pathway.

In order to further demonstrate that TGX221-induced apoptosis was mediated by ER stress, we examined the expression levels of ER stress markers, the heat shock protein family (GRP78), and other related proteins. As shown in Fig. 5I, GRP78, p-PERK, and CHOP were significantly upregulated. The expression level of ATF4 also increased significantly, indicating that TGX221 induced ER stress. Although the primary purpose of the unfolded protein response (UPR) is to restore ER homeostasis, ATF4-CHOP activation can induce the apoptotic pathway if ER stress is irreversible.[25] To further prove that ER stress promoted apoptosis, we selected ER stress inhibitor TUDCA for analysis. As shown in Fig. 5G, the pro-apoptotic effect of TGX221 was partially reversed by inhibiting ER stress with TUDCA. These results confirmed that TGX221 induced ER stress-mediated apoptosis, which was mediated by the PERK/ATF4/CHOP pathway.

3.6 *In vivo* imaging analysis

In order to evaluate the targeting effect of the folate-targeted liposomes on prostate cancer, we established a PC-3 cell

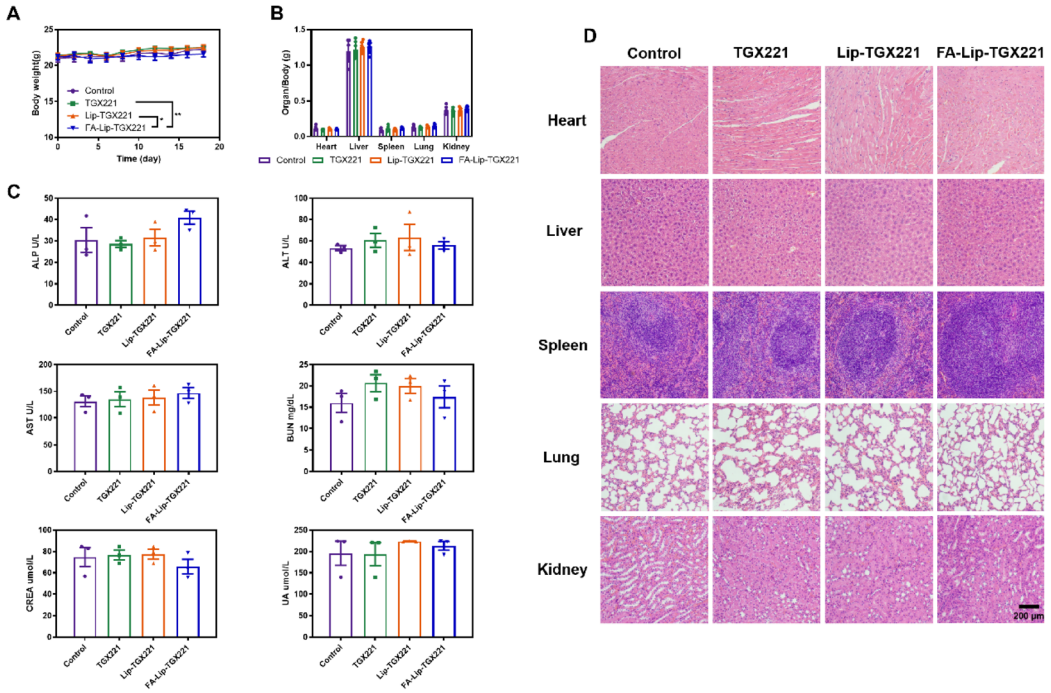

Fig. 8 *In vivo* biosafety assessment. Changes in (A) body weight and (B) visceral body weight in PC-3 tumor bearing mice. (C) Blood biochemical indicators include liver function indicators (ALT, AST, and ALP) and renal function indicators (CREA, BUN, and UA). (D) Representative H&E staining images of major organs (heart, lung, liver, spleen, and kidney) in different groups [scale = 200 μm] (mean ± SD, $n = 7$, $^{*}P < 0.05$, or $^{**}P < 0.01$).

tumor-bearing mouse model. DiR was selected as the fluorescent probe to prepare fluorescent liposomes FA-Lip-DiR and Lip-DiR to observe the biological distribution *in vivo* of the liposomes to study the active targeted delivery of drugs. As shown in Fig. 6A and C, stronger fluorescence intensity was detected in the FA-Lip-DiR group than in the Lip-DiR group, and fluorescence in the FA-Lip-DiR group persisted 48 hours after administration. However, the fluorescence of free DiR was hardly observed in the tumor. In addition, *in vitro* fluorescence images of tumor tissues and major organs also confirmed that stronger fluorescence was observed in tumors in the FA-Lip-DiR group (Fig. 6B and D). These results indicated that the folate-targeted liposomes had a strong tumor targeting ability and accumulated in tumor sites over time.

3.7 Anti-tumor efficacy *in vivo*

The*in vivo* antitumor effect was evaluated in PC-3 cell tumor-bearing mice after intravenous administration of different drug preparations (Fig. 7A). The tumor image, tumor growth curve and tumor weight are shown in Fig. 7B–D. It can be seen that after 2 weeks of treatment, the tumor grew rapidly in the control group, but was suppressed in the drug treatment group. Notably, compared with Lip-TGX221, FA-Lip-TGX221 showed a better antitumor effect, suggesting that FA-Lip-TGX221 increased the accumulation of TGX221 in the tumor area through the active targeting of FA, thereby enhancing the inhibition of tumor growth.

Subsequently, we detected the expression of related proteins by western blot. As shown in Fig. 7E and S6,† the expressions of p110β, p-Akt and Bcl-2 were significantly lower in the FA-Lip-TGX221 group than in the control group, while the expression of PTEN was increased. These results suggested that FA-Lip-TGX221 could induce apoptosis of PC-3 cells by inhibiting the proteins related to the PI3K-Akt signaling pathway, thereby reducing the proliferation of PC-3 cells. In addition, the expressions of GRP78, CHOP and ATF4 in PC-3 cells were significantly higher in the FA-Lip-TGX221 group than in the control group, indicating that FA-Lip-TGX221 induced the apoptosis of PC-3 cells by activating ER stress.

Next, antitumor studies were further carried out using H&E, Ki67, and TUNEL staining (Fig. 7F). H&E staining results showed that different degrees of apoptosis appeared in the administration groups, accompanied by nuclear contraction and nuclear rupture. Immunohistochemical analysis of Ki67 staining used to assess tumor proliferation demonstrated a significant decrease in the number of Ki67 positive cells expressed in the FA-Lip-TGX221 group. In addition, TUNEL analysis demonstrated that at equivalent doses, tumor cell apoptosis in the FA-Lip-TGX221 group was greater than that in the TGX221 group. These results suggested that FA-Lip-TGX221 exerted a greater antitumor effect than Lip-TGX221, which might be because folate-targeted liposomes could be absorbed through folate receptor-mediated endocytosis, thereby enhancing drug internalization.

3.8 *In vivo* biosafety

Biosafety is also an important index to evaluate drug delivery systems based on liposomes. As shown in Fig. 8A and B, there

was no significant difference in body weight or visceral body weight between the liposome group and the control group (normal saline), confirming the good biocompatibility of the liposomes.

In addition, biochemical blood indices of tumor-bearing mice were further investigated. As shown in Fig. 8C, liver function indices such as alanine aminotransferase (ALT), aspartate aminotransferase (AST) and alkaline phosphatase (ALP), and renal function indices such as creatinine (CREA), urea nitrogen (BUN) and uric acid (UA) showed no obvious abnormalities, indicating that FA-Lip-TGX221 had no adverse effects on the liver and kidney.

Finally, H&E staining was performed on the major organs (heart, lung, liver, spleen and kidney) for safety evaluation (Fig. 8D). The results showed that there was no obvious histopathological damage in all groups, indicating that this liposomal system was a safe drug carrier with good biocompatibility.

4. Conclusion

In conclusion, we have successfully developed a kind of folate-targeted pH-sensitive liposome encapsulating TGX221, an effective specific inhibitor of PI3K, as a model drug (FA-Lip-TGX221) for the treatment of prostate cancer. In FA-Lip-TGX221, FA was connected to Chol to form the targeting component (FA-PEG-CHEMS) *via* an ester bond, which was different from most FA-modified liposomes. As Chol is generally used to stabilize liposomes, the structure of the liposomes will be easily destructed to release the drug loaded when FA-PEG-CHEMS is broken under acidic conditions in the tumor microenvironment.

FA-Lip-TGX221 presented a uniform spherical shape with an average particle size of less than 200 nm, and exhibited good stability and pH-responsive drug release ability. Both *in vitro* and *in vivo* experiments demonstrated that FA-Lip-TGX221 had a significant inhibitory effect on proliferation of PC-3 cells. Mechanism studies indicated that this delivery system could effectively inhibit PI3K/Akt signaling pathway transduction and induce ER stress, thereby inhibiting tumor cell proliferation and promoting apoptosis. Hence, this active targeted drug delivery system shall provide an important reference for the treatment of advanced prostate cancer and deserves further study.

Data availability

All data are presented in the manuscript and the ESI.† No additional data are available.

Author contributions

J. Cen and S. Duan conceived and designed the experiments and supervised the project. W. Xu, X. Li, F. He, H. Zhao, J. Wu, M. Li, X. Dai, Y. Li and X. Hu performed all the experiments. X. Li carried out the validation work. P. Guo revised the manuscript. All authors analyzed and discussed the data. J. Cen and S. Duan wrote and revised the manuscript. W. Xu, X. Li and F. He contributed equally to this paper.

Conflicts of interest

The authors declare that they have no known competing financial interests or personal relationships that could influence the work reported in this study.

Acknowledgements

This work was kindly supported by the Key Research and Development Projects of Henan Province (222102310453, 232102311170, and 232102310504).

References

1 R. J. Rebello, C. Oing, K. E. Knudsen, *et al.*, Prostate cancer, *Nat. Rev. Dis. Primers*, 2021, **7**(1), 9.
2 C. Kaittanis, C. Andreou, H. Hieronymus, *et al.*, Prostate-specific membrane antigen cleavage of vitamin B9 stimulates oncogenic signaling through metabotropic glutamate receptors, *J. Exp. Med.*, 2018, **215**(1), 159–175.
3 A. D. Whale, L. Colman, L. Lensun, *et al.*, Functional characterization of a novel somatic oncogenic mutation of PIK3CB, *Signal Transduction Targeted Ther.*, 2017, **2**(1), 17063.
4 Z. Zhang, L. Hou, Z. Yu, *et al.*, Biomimetic Small-Molecule Self-Assembly of PI3K inhibitor integrated with immunomodulator to amplify anticancer efficacy, *Chem. Eng. J.*, 2022, **433**, 133747.
5 N. Haddadi, Y. Lin, G. Travis, *et al.*, PTEN/PTENP1: 'Regulating the regulator of RTK-dependent PI3K/Akt signalling', new targets for cancer therapy, *Mol. Cancer*, 2018, **17**(1), 37.
6 G. Hoxhaj and B. D. Manning, The PI3K–AKT network at the interface of oncogenic signalling and cancer metabolism, *Nat. Rev. Cancer*, 2020, **20**(2), 74–88.
7 D. A. Fruman, H. Chiu, B. D. Hopkins, *et al.*, The PI3K Pathway in Human Disease, *Cell*, 2017, **170**(4), 605–635.
8 M. Marqués, R. Tranchant, B. Risa-Ebrí, *et al.*, Combined MEK and PI3K/p110β Inhibition as a Novel Targeted Therapy for Malignant Mesothelioma Displaying Sarcomatoid Features, *Cancer Res.*, 2020, **80**(4), 843–856.
9 Y. Zhang, P. Kwok-Shing Ng, M. Kucherlapati, *et al.*, A Pan-Cancer Proteogenomic Atlas of PI3K/AKT/mTOR Pathway Alterations, *Cancer Cell*, 2017, **31**(6), 820–832e3.
10 R. Sano and J. C. Reed, ER stress-induced cell death mechanisms, *Biochim. Biophys. Acta, Mol. Cell Res.*, 2013, **1833**(12), 3460–3470.
11 Z. Jin, W. Yan, M. Qu, *et al.*, Cinchonine activates endoplasmic reticulum stress-induced apoptosis in human liver cancer cells, *Exp. Ther. Med.*, 2018, **15**(6), 5046–5050.
12 Z. Shen, L. Yin, H. Zhou, *et al.*, Combined inhibition of AURKA and HSF1 suppresses proliferation and promotes apoptosis in hepatocellular carcinoma by activating

endoplasmic reticulum stress, *Cell. Oncol.*, 2021, **44**(5), 1035–1049.
13 H. D. Ryoo, Long and short (timeframe) of endoplasmic reticulum stress-induced cell death, *FEBS J.*, 2016, **283**(20), 3718–3722.
14 L. R. Palam, T. D. Baird and R. C. Wek, Phosphorylation of eIF2 Facilitates Ribosomal Bypass of an Inhibitory Upstream ORF to Enhance CHOP Translation, *J. Biol. Chem.*, 2011, **286**(13), 10939–10949.
15 I. C. Salaroglio, E. Panada, E. Moiso, *et al.*, PERK induces resistance to cell death elicited by endoplasmic reticulum stress and chemotherapy, *Mol. Cancer*, 2017, **16**(1), 91.
16 H. Zinszner, M. Kuroda, X. Wang, *et al.*, CHOP is implicated in programmed cell death in response to impaired function of the endoplasmic reticulum, *Genes Dev.*, 1998, **12**(7), 982–995.
17 B. Ma, H. Zhang, Y. Wang, *et al.*, Corosolic acid, a natural triterpenoid, induces ER stress-dependent apoptosis in human castration resistant prostate cancer cells *via* activation of IRE-1/JNK, PERK/CHOP and TRIB3, *J. Exp. Clin. Cancer Res.*, 2018, **37**(1), 210.
18 S. A. Oakes and F. R. Papa, The Role of Endoplasmic Reticulum Stress in Human Pathology, *Annu. Rev. Pathol.:Mech. Dis.*, 2015, **10**(1), 173–194.
19 J. Ni, Q. Liu, S. Xie, *et al.*, Functional Characterization of an Isoform-Selective Inhibitor of PI3K-p110β as a Potential Anticancer Agent, *Cancer Discovery*, 2012, **2**(5), 425–433.
20 H.-F. Zhao, J. Wang, H.-R. Jiang, *et al.*, PI3K p110β isoform synergizes with JNK in the regulation of glioblastoma cell proliferation and migration through Akt and FAK inhibition, *J. Exp. Clin. Cancer Res.*, 2016, **35**(1), 78.
21 C. He, S. Duan, L. Dong, *et al.*, Characterization of a novel p110β-specific inhibitor BL140 that overcomes MDV3100-resistance in castration-resistant prostate cancer cells, *Prostate*, 2017, **77**(11), 1187–1198.
22 S. P. Jackson, S. M. Schoenwaelder, I. Goncalves, *et al.*, PI 3-kinase p110β: a new target for antithrombotic therapy, *Nat. Med.*, 2005, **11**(5), 507–514.
23 R. Xu, Y. Zhang, A. Li, *et al.*, LY-294002 enhances the chemosensitivity of liver cancer to oxaliplatin by blocking the PI3K/AKT/HIF-1α pathway, *Mol. Med. Rep.*, 2021, **24**(1), 508.
24 R. Chen, Y. Zhao, Y. Huang, *et al.*, Nanomicellar TGX221 blocks xenograft tumor growth of prostate cancer in nude mice, *Prostate*, 2015, **75**(6), 593–602.
25 S. Shah, V. Dhawan, R. Holm, *et al.*, Liposomes: Advancements and innovation in the manufacturing process, *Adv. Drug Delivery Rev.*, 2020, **154–155**, 102–122.
26 S. G. Antimisiaris, A. Marazioti, M. Kannavou, *et al.*, Overcoming barriers by local drug delivery with liposomes, *Adv. Drug Delivery Rev.*, 2021, **174**, 53–86.
27 O. C. Farokhzad and R. Langer, Impact of Nanotechnology on Drug Delivery, *ACS Nano*, 2009, **3**(1), 16–20.
28 M. Dymek and E. Sikora, Liposomes as biocompatible and smart delivery systems – the current state, *Adv. Colloid Interface Sci.*, 2022, **309**, 102757.
29 Y. Barenholz (Chezy), Doxil®—The first FDA-approved nano-drug: Lessons learned, *J. Controlled Release*, 2012, **160**(2), 117–134.
30 N. Filipczak, J. Pan, S. S. K. Yalamarty, *et al.*, Recent advancements in liposome technology, *Adv. Drug Delivery Rev.*, 2020, **156**, 4–22.
31 Y. He, M. M. Sun, G. G. Zhang, *et al.*, Targeting PI3K/Akt signal transduction for cancer therapy, *Signal Transduction Targeted Ther.*, 2021, **6**(1), 425.
32 K. M. Au, A. Satterlee, Y. Min, *et al.*, Folate-targeted pH-responsive calcium zoledronate nanoscale metal-organic frameworks: Turning a bone antiresorptive agent into an anticancer therapeutic, *Biomaterials*, 2016, **82**, 178–193.
33 Y. I. Park, S.-H. Kwon, G. Lee, *et al.*, pH-sensitive multi-drug liposomes targeting folate receptor β for efficient treatment of non-small cell lung cancer, *J. Controlled Release*, 2021, **330**, 1–14.
34 Q. Guo, L. Zhang, M. He, *et al.*, Doxorubicin-loaded natural daptomycin micelles with enhanced targeting and anti-tumor effect *in vivo*, *Eur. J. Med. Chem.*, 2021, **222**, 113582.
35 Z.-A. Zhang, X. Xin, C. Liu, *et al.*, Novel brain-targeted nanomicelles for anti-glioma therapy mediated by the ApoE-enriched protein corona *in vivo*, *J. Nanobiotechnol.*, 2021, **19**(1), 453.